Comparison of the Performance of Cu-CeO_2-YSZ and Ni-YSZ Composite SOFC Anodes with H_2, CO, and Syngas

Olga Costa-Nunes, Raymond J. Gorte, and John M. Vohs*

Department of Chemical & Biomolecular Engineering,
University of Pennsylvania,
Philadelphia, PA, 19104 USA

Abstract

In this study the performance of a solid oxide fuel cell (SOFC) with Cu-CeO_2-yttria-stabilized zirconia (YSZ) was compared to an SOFC with Ni-YSZ anode while operating on H_2, CO, and syngas fuels. Cells with Cu-CeO_2-YSZ anodes exhibited similar performance when operating on H_2 or CO fuels, while cells with Ni-YSZ anodes exhibited substantially lower performance when operating on CO compared to H_2. Enhancing the catalytic activity of the Cu-CeO_2-YSZ anodes by adding Co was shown to produce cells that exhibited higher performance when operating on CO compared to H_2 at 973 K. The effect of fuel concentration and dilution on cell performance was also investigated and it was found that the kinetics of the oxidation of H_2 are positive order in P_{H_2} for Cu-CeO_2-YSZ anodes and nearly zero order in P_{H_2} for Ni-YSZ anodes. The oxidation of CO on Cu-CeO_2-YSZ anodes was also found to exhibit positive order in P_{CO}. It was also demonstrated that dilution of H_2 by H_2O had little effect on the kinetics of H_2 oxidation on both the Cu-CeO_2-YSZ and Ni-YSZ anodes.

Keywords: solid oxide fuel cells, anodes

* Corresponding author. Tel.: 01 215 898 6318, fax: 01 215 573 2093
e-mail address: vohs@seas.upenn.edu (J. Vohs)

1. Introduction:

In many of the proposed applications for solid oxide fuel cells (SOFCs) the system will be powered using syngas (i.e. a mixture of H_2, CO, and N_2) produced via reforming of hydrocarbons. It is, therefore, important to understand how fuel composition and the presence of diluents such as N_2 and reaction products such as CO_2 and H_2O affect SOFC performance. While most studies of SOFCs in the literature report performance characteristics for operation on humidified H_2, there have been some studies that have looked at the effect of fuel composition [1-4]. For example, it has been reported that for SOFCs with conventional Ni-YSZ cermet anodes, the rate of the electrochemical oxidation of H_2 is 2-3 times greater than that of CO [1,2]. Jiang & Virkar found that for a cell with a Ni-YSZ anode that exhibited a maximum current density of 1.7 Wcm^{-2} at 1073 K while operating on H_2, had a maximum current density of only 0.3 W cm^{-2} when the fuel was switched to a 45%/55% CO/CO_2 mixture.

While CO by itself is a poor fuel for Ni-based anodes it can be used to produce more H_2 via the water gas shift reaction (WGS),

$$CO + H_2O \rightarrow CO_2 + H_2,$$

which is also catalyzed by Ni. For fuels that have high CO contents, for example syngas produced from coal, H_2O may need to be added to the fuel in order to effectively utilize the CO. Of course for cells that operate at high conversion the fuel will become diluted in both CO_2 and H_2O. Thus, it is important to understand how the partial pressure of these species in the fuel affects the kinetics of the anode reactions. In the case of water, there have been several reports in the literature that suggest that it has a promoting effect on the rate of electrochemical oxidation of H_2 [5-9].

While much is already known about how syngas composition and the presence of reaction products and other diluents affects the performance of SOFCs with Ni-YSZ anodes, relatively little is known about how these factors affect the performance of anodes with other formulations. We have developed SOFC anodes that are composites of Cu, CeO_2 and yttria-stabilized zirconia (YSZ). In this anode formulation the CeO_2 acts primarily as an oxidation catalyst, while the Cu provides electronic conductivity [10,11]. Although these anodes were initially developed for the direct utilization of hydrocarbons without the need for reforming [12-15], they can also operate on syngas and may have some advantages, such as sulfur tolerance, compared to Ni-based anodes for this fuel [16]. The goal of this study was, therefore, to compare the performance of SOFCs with Ni-YSZ and Cu-CeO_2-YSZ anodes while operating on H_2, CO and syngas and to evaluate how the presence of diluents and reaction products affects their performance.

2. Experimental

The anode and cathode supported cells used in this study and their characteristics are summarized in Table 1. Cathode supported cells were used in studies comparing the performance of Cu-CeO_2-YSZ and Ni-YSZ anodes. These cells were supported on a LSF-YSZ composite cathode, used YSZ as the electrolyte, and had either Cu-CeO_2-YSZ (cell 1) or Ni-YSZ (cell 2) composite anodes. The cells were 1 cm in diameter and produced via tape casting using methods that have been previously described in detail [10]. A porous YSZ cathode and a dense electrolyte layer for each cell were formed by casting a tape containing yttria-stabilized zirconia (YSZ) with graphite and polymethylmethacrylate (PMMA) pore formers over a pure YSZ green tape. A porous YSZ anode layer was then

added by painting a YSZ slurry containing the pore formers onto the exposed side of the electrolyte tape. The three-layer green tape was then calcined at 1823 K, producing a 60 μm thick, dense YSZ layer between 600 and 200 μm thick porous YSZ layers. LSF was added to the 600 μm thick porous YSZ layer in order to form the cathode. This was accomplished using sequential impregnations of a solution containing La, Sr and Fe nitrates ($La(NO_3)_3.6H_2O$, Alfa Aesar, ACS 99.9%; $Sr(NO_3)_2$ Alfa Aesar, ACS 99.0%; $Fe(NO_3)_3.9H_2O$ Alfa Aesar, ACS 98+%) in a 0.8:0.2:1 molar ratio. LSF-YSZ composite cathodes with a 40:60 molar composition were obtained after calcination at 1123 K. A more detailed description of the fabrication of LSF-YSZ cathodes using this approach can be found elsewhere [17].

The anode composites used in this study had an area of 0.35 cm^2. The Cu-CeO_2-YSZ anodes (15 wt% Cu and 11 wt % CeO_2) were prepared by impregnating the 200 μm thick porous YSZ layer with aqueous solutions of $Ce(NO_3)_3$ and $Cu(NO_3)_2$ followed by calcination at 723 K to form the oxides. The copper oxide was reduced to Cu metal during cell activation in H_2. Ni-YSZ anodes (38 wt % Ni) were produced in a similar manner using impregnation with aqueous Ni $(NO_3)_2$. Since the Cu-CeO_2-YSZ and Ni-YSZ anodes were fabricated using identical porous YSZ layers and impregnation procedures they have similar porosities and microstructures. Ag paste and an Ag mesh were used to make electrical contact with the cathode and Au paste and an Au mesh were used for the anode. For performance testing each cell was sealed onto a 1.0 cm diameter alumina tube using a zirconia-based adhesive (Aremco, Ultra-Temp 516) and then the entire cell was placed

inside a furnace and heated 2 $Kmin^{-1}$ to 973 K while exposing the cathode to air and the anode to H_2.

Two additional anode supported cells with anode thicknesses of 300 μm and 3 mm were also used in this study. These cells were prepared using procedures similar to those described above, except for the fact that thick porous YSZ layer was used as the anode, and thin layer as the cathode. The cell with the 3 mm anode (cell 4) was used to study diffusional limitations, while the cell with the 300 μm anode was used to study the effect of the addition of a cobalt co-catalyst (cell 3). For this latter cell, cobalt was added by impregnation using a solution containing Cu and Co nitrates in a 1:1 molar ratio.

During testing each fuel cell was operated at atmospheric pressure and mass flow controllers were used to adjust the flow rates and composition of the various gasses (i.e. H_2, CO, CO_2, He, and N_2) sent to the anode. The cathode was left exposed to the atmosphere. The syngas used in this study contained 25% H_2, 25% CO and 50% N_2. The total flow rate of fuel to the anode was held constant at 200 $mLmin^{-1}$. For this flow rate the fuel conversion within the cell was less than 5% for all fuel compositions and current densities studied. A temperature controlled water bubbler was used to introduce water into the fuel. All impedance data were recorded in the galvanostatic mode using a Gamry Instruments impedance spectrometer.

3. Results & Discussion:

3.1. Cell Performance in Syngas: Comparison Between Cu-Ceria and Ni

Voltage versus current (V-I) curves for the cathode-supported cells with Cu-CeO_2-YSZ (A) and Ni-YSZ (B) anodes at 973 K while operating with H_2, CO, and syngas are presented in Figure 1. Impedance spectra while operating at a current density of 150 mA cm^{-2} are also displayed for each cell in this figure. The Cu-Ceria-YSZ cell (cell 1) exhibited an open circuit voltage (OCV) of 1.2 V for all fuels tested. This value is due to the fact that non-humidified fuels were used for this cell. The maximum power density for this cell when running on H_2 was 305 mW cm^{-2} and the cathode-to-anode impedance spectrum contains two arcs centered at approximately 1 kHz and 4 Hz. In a previous study of LSF-YSZ cathodes of the same structure as that used here it was shown that they have an area specific resistance (ASR) of ~0.1 ohm-cm^2 and a characteristic frequency of 1 kHz in impedance spectrum [17]. Thus, the 1 kHz arc in the impedance spectrum for the cell 1 can be assigned to the cathode. The large arc centered at 4 Hz is, therefore, due primarily to processes occurring on the anode.

The OCV for cell 2 with the Ni-YSZ anode operating on humidified H_2 (P_{H_2O} = 0.03 atm) was 1.1 V which is in agreement with the Nernst equation. The maximum current density for this cell with H_2 was 136 mW cm^{-2} which is significantly less than that obtained for the Cu-CeO_2-YSZ cell. The impedance spectrum shows that this lower performance is due primarily to a high ohmic loss in this cell of 1.1 ohm-cm^2. This can be attributed to the microstructure of the anode. In a previous study of Cu-CeO_2 anodes it was shown that the impregnated ceria forms an even coating on the surface of the porous YSZ [10] which in addition to providing catalytic activity enhances the electrical conduction path throughout the anode. In cells without ceria the contact between the YSZ and the metal is not as good

because the metal tends not to wet the surface of the YSZ. Thus for the Ni-YSZ cell, the high ohmic loss can be attributed to an increase in the effective thickness of the electrolyte due to poor distribution of the impregnated Ni layer.

The data in Figure 1 for operation on the various fuels illustrate several important points. For the Cu-CeO_2-YSZ cell, the performance when using either H_2 or CO is nearly identical. Only slightly lower performance was obtained when running on syngas which can be attributed to dilution of the combustible portion of the fuel in N_2. This is in contrast to the reactivity trends observed for the Ni-YSZ cell for which the performance when running on CO was substantially less than that for H_2. The maximum power densities for this cell were 136, 120 and 73 mW cm^{-2} for H_2, syngas and CO, respectively. Thus for the Ni-YSZ cell, the maximum power density when operating on CO was only 50 % of that when operating on H_2. The poor performance on CO for this cell is also reflected by the large increase in the anode arc in the impedance spectrum upon switching from H_2 to CO. This result is consistent with that reported previously by Jiang and Virkar [4] who also observed poor performance for cells with Ni-YSZ cermet anodes when running on CO. Also note that the performance of the Ni-YSZ cell on syngas is only slightly less than that when using H_2 and the impedance spectra for operation on these two fuels are similar. This demonstrates that when running on dry syngas only the H_2 component of the fuel is being oxidized.

Since Ni by itself is a good CO oxidation catalyst, the low performance of the Ni-YSZ cell for this fuel cannot be ascribed to poor catalytic activity within the anode. One possible explanation for the poor performance on CO is that the combustion reactions involve fuel molecules adsorbed on the oxide surface at or near the three-phase boundary

(TPB). Hydrogen adsorbs dissociatively on Ni and it is possible that the H atoms "spillover" onto the YSZ where oxidation takes place. This type of spillover process for H atoms on metals supported on oxides is well documented in the catalysis literature [19]. In contrast to H atoms, spillover of CO adsorbed on a metal to an oxide support generally does not occur. One would not expect to observe these effects for a Cu-CeO_2-YSZ anode, since in this case the metal is largely inert as evidenced by the fact that substitution of Cu with Au gives identical electrode performance [20]. Thus for the Cu-CeO_2-YSZ anode, the reactions appear to take place on the ceria which is active for both H_2 and CO oxidation.

It is known that the redox properties of ceria can be enhanced by the addition of a catalytic metal and indeed we have observed enhanced anode performance by the addition of precious metals to the ceria [21] and by adding Co to the Cu phase [22]. In the case of the Cu-Co bimetallic anodes, the surface of the metallic phase appears to be primarily Cu, as demonstrated by a low susceptibility for carbon formation when running on hydrocarbons, but with some Co dissolved within the Cu, as evidenced by improved performance for H_2 and CH_4 [22]. In order to determine whether the enhancements associated with Co might extend to CO, the performance of a cell in which Co, in addition to Cu and CeO_2, was impregnated into the anode (cell 3) was measured. Current voltage curves and impedance spectra obtained form this cell as a function of fuel composition are displayed in Figure 2. The addition of Co did produce an increase in performance and the maximum power densities for this cell were approximately 20% higher than those obtained from the Cu-CeO_2 cell. For operation on humidified H_2, syngas, and CO the maximum power densities were 310, 360, and 370 mW cm^{-2}, respectively at 973 K. Thus, cell 3 exhibited higher performance when operating on CO compared to H_2. It is noteworthy that

the performance of the cell with the Cu-Co-CeO_2-YSZ anode, even with a relatively thick electrolyte and operating at lower temperatures, exhibits a performance in CO that rivals that of some of the best Ni-YSZ cells operating on H_2 at 1073 K reported in the literature [4].

The impedance spectrum in Figure 2 also shows that cell 3 has an ohmic loss of 0.35 ohm cm^2. Assuming a conductance of 0.02 S cm^{-1} for YSZ at 973 K [18], the ASR of the 60 μm electrolyte layer should be ~0.3 ohm cm^2, which is close to the experimental value obtained here. The higher value of 0.6 ohm-cm^2 ohmic loss measured for cell 1 (Figure 1 panel (A)) can be attributed difference in metal content between cells 1 and 3, which were 15 and 30 wt %, respectively. This variation could have lowered the electronic conductivity in the case of cell 1 resulting in a higher ohmic resistance.

When considering how fuel composition affects cell performance one must recognize that in addition to CO, H_2 and N_2, reformed hydrocarbon fuels are likely to contain small amounts of hydrocarbon impurities. It is therefore important to evaluate the propensity for these impurities to foul the anode via carbon deposition and their effect on the kinetics of the oxidation of CO and H_2. The stability of Cu-CeO_2-YSZ anodes in the presence of hydrocarbons and their ability to directly utilize hydrocarbon fuels has previously been demonstrated [12-15]. Thus, carbon fouling due to hydrocarbon impurities should not be an issue for this anode formulation. The effect of hydrocarbon impurities on the performance of these anodes when operating on syngas, however, has yet to be evaluated. We therefore carried out a set of experiments with cell 1 using H_2 and CO fuels containing 10% n-C_4H_{10}. The results of this study are shown in Figure 3. For comparison

purposes, I-V curves for cell 1 running on pure H_2, CO, and n-C_4H_{10} are also included in the figure. Due to the slower kinetics for the oxidation of the n-C_4H_{10} the cell performance is significantly lower when running with this fuel compared to H_2 or CO. This result is consistent with that reported in previous studies [23]. For CO and H_2 fuels the addition of 10% n-C_4H_{10} resulted in only a modest decrease in cell performance suggesting that the primary effect of adding butane was to dilute the CO and H_2.

3.2. Influence of Fuel Concentration

Concentration is another variable that will affect the kinetics of the electrochemical oxidation of the fuel. Since in a large cell or a stack that operates at high fuel utilization the fuel will be diluted by the oxidation products, CO_2 and H_2O, it is important to understand how this will affect performance. To investigate this, the performance of cells with Ni-YSZ (cell 2) and Cu-CeO_2-YSZ (cell 1) anodes were measured as a function of fuel composition at 973 K. In this study the cell performance was measured for a fuel consisting of H_2 diluted in both He and H_2O. For the Cu-CeO_2-YSZ cell, the effect of diluting CO in an inert gas and CO_2 was also studied.

Figure 4 displays V-I curves for the Cu-CeO_2-YSZ (panel A) and Ni-YSZ (panel B) cells as a function of H_2 partial pressure at 973 K. In this set of experiments the partial pressure of H_2O in the fuel was held constant at 0.03 atm and the flow rates of H_2 and He were adjusted to give H_2 partial pressures of 0.1, 0.5, and 0.97 atm. The corresponding Nernst potentials for these fuel compositions are 1.1, 1.07, and 1.0 V, respectively, which agree well with the measured OCVs for both cells. The cathode and electrolyte losses for these cells can be approximated using the previously measured value of the ASR of the

LSF-YSZ cathode (0.1 ohm-cm^2) [17] and estimates of the effective ASR of the electrolyte obtained form the impedance spectra in Figure 1. The anode overpotentials as a function of current density for each fuel were estimated from the difference in the OCV, the operating potential, and the voltage losses associated with the cathode and electrolyte. These estimates are also displayed in Figure 4.

For the Cu-CeO_2-YSZ cell, the anode performance depends on the H_2 partial pressure. This kinetics of the anode reaction for this cell is positive order in P_{H_2} as reflected by the decrease in the anode overpotential with increasing P_{H_2}. With the Ni-YSZ anode, the effect is much less pronounced. For current densities less than 190 mA cm^{-2}, there is a negligible change in the anode overpotential as P_{H_2} is increased from 0.1 to 0.97 atm, indicating that the reaction is essentially zero order in P_{H_2}. From 190 to 500 mA cm^{-2}, changing the pressure from 0.97 to 0.5 atm still had no effect on the anode overpotential; however, there was a precipitous drop in the overpotential at lower partial pressures. We currently do not completely understand the reason for this drop; however, it cannot be attributed to diffusional limitations since the overall cell conversion was less than 5% and a similar drop was not observed at higher temperatures where the performance levels were much higher. One possible explanation for this feature is that the oxidation of H_2 on the Ni-based anode exhibits complex kinetics and there is a change in the rate limiting step at low H_2 concentrations.

Figure 5 displays V-I curves as a function of the partial pressure of the fuel at 973 K for the Cu-CeO_2-YSZ cell (cell 1) while operating on dry CO or CO diluted in either N_2 or CO_2 (panel A). Plots of the anode overpotentials are also included in the figure. Dilution

of the CO in N_2 had no appreciably effect on the OCV of 1.1 V. At current densities lower than 100 mA cm^{-2} dilution also had little effect on the anode overpotential, while at higher current densities it caused a significant increase in the overpotential. Although this dependence on current density may indicate complex kinetics, overall these results show that the anode reaction is positive order in P_{CO}.

Diluting the CO in 50% CO_2 caused the OCV to decrease to 0.97 V as predicted by the Nernst equation. Dilution in CO_2 also resulted ~0.1 V smaller anode overpotentials compared to dilution in N_2. Since the V-I curves for these two fuel compositions are parallel to each other, this difference appears to be due primarily to a reduction in the OCV rather than inhibition of the rate of reaction on the anode due to the presence of CO_2. It is useful to compare this result to that reported previously by Jiang & Virkar who also studied how dilution of CO in CO_2 affects the performance of an SOFC with a Ni-YSZ anode [4]. For operation at 1073 K they found that as P_{CO} was decreased from 1 to 0.44 atm by diluting in CO_2 the maximum power density decreased by 60%. In the present study decreasing P_{CO} from 1 to 0.5 atm by diluting in CO_2 produced only a 27% decrease in the maximum current density at 973 K. These results again serve to illustrate the differences in the kinetics of the oxidation of CO on Cu-CeO_2-YSZ compared to Ni-YSZ and the superiority of the former for this reaction.

For hydrocarbon fuel, dilution has relatively little effect on the performance as has been reported previously for the Cu-CeO_2-YSZ cell running in n-butane [23]. In this earlier study, it was also shown that the oxidation products acted primarily as diluents, so that the presence of H_2O and CO_2 did not significantly affect the power density. Additionally it

should be noted that thermodynamics predicts that P_{O_2} should not change significantly with conversion when hydrocarbons are used as fuels; however, in the case of H_2 this change is more substantial.

The influence of P_{H_2O} on the kinetics of the H_2 oxidation reaction on the anode was also investigated. Figure 6 displays V-I curves obtained from the Cu-CeO_2-YSZ (cell 1) and Ni-YSZ (cell 2) cells at 973 K as a function of P_{H_2O}. In this series of experiments P_{H_2} was held constant at 0.1 atm and the N_2 and H_2O flow rates were adjusted to give P_{H_2O} values of 0, 0.03, and 0.5 atm (only data for 0.03 and 0.5 atm were collected for the Ni-YSZ cell). Panel A in the figure shows that for the Cu-CeO_2-YSZ cell increasing P_{H_2O} lowered the OCV as predicted by the Nernst equation. At low current densities this caused a decrease in the cell performance with increasing P_{H_2O}. At high current densities, however, the V-I curves were largely independent of P_{H_2O} indicating that water had little effect on the kinetics of the oxidation reaction for this anode composition. Examination of the anode overpotentials rather than just the cell V-I curves leads to a similar conclusion. For example, at a current density of 400 mA cm^{-2} the anode overpotential (calculated in a manner similar to that described above and taking into account the water produced in the cell) was 0.4 volts for P_{H_2O} = 0 and 0.03 and 0.5 atm. This result is in contrast to that obtained for the Ni-YSZ cell at 973 K where the addition of 0.5 atm of H_2O produced a noticeable decrease in current density for current densities greater than 175 mA cm^{-2}. Again note the pronounced change in slope at intermediate current densities suggesting complex kinetics for the H_2 oxidation reaction. This result indicates that at 973 K the oxidation of H_2 on Ni-YSZ anodes is slightly negative order in the water concentration.

Data for the effect of P_{H_2O} on the performance of the Ni-YSZ cell while operating on H_2 at 1073 K is also presented in Figure 6. At this temperature the addition of 0.5 atm of water had little effect on the cell performance except for a slight lowering of the OCV. Also note that at this temperature the V-I curve is almost linear and does not contain the pronounced change in slope at intermediate current densities. Since the diffusivity of a gas is only a weak function of temperature, this result further demonstrates that the change in slope in the V-I curve observed at 973 K is not due to diffusional limitations. The results obtained at 1073 K are in agreement with those reported previously for Jiang and Virkar who also found that other than lowering the OCV, the addition of water to H_2 fuel had little effect on the kinetics of the anode reaction for an SOFC with a Ni-YSZ anode [4]. Both of these studies, therefore, demonstrate that for operation on H_2 the addition of water has a relatively small effect on the kinetics of the oxidation reaction on the anode. These results do not agree with previous reports that addition of H_2O increases the rate of H_2 oxidation on the anode [5-9] and indicate that the rate expression for this reaction is nearly zero order in P_{H_2O} at 1073 K and slightly negative order in P_{H_2O} at 973 K.

3.3. Diffusional Limitations.

In assessing the effect of fuel concentration and the addition of diluents on the performance of the fuel cells it is important to be able to distinguish between effects caused by changes in the kinetics of the anode oxidation reactions and those resulting from diffusional limitations in the porous anode. In the preceding analysis we have argued that the changes were due exclusively to the anode kinetics and not diffusional limitations. This

assumption can be justified using a simple Fick's Law analysis. Diffusional limitations will become important when the fuel concentration at or near the three phase boundary, C_{TPB}, deviates significantly from that at the surface of the anode, $C_{surface}$. If one assumes a homogenous anode structure and that electrochemical oxidation at the TPB is the sole reaction, the deviation of C_{TPB} from $C_{surface}$ can be estimated using the following equation

$$i = nF * [(D_{FUEL,EFF}/\delta) * (C_{surface} - C_{TPB})] \qquad (1)$$

where i is the current density, n is the number of electrons produced by the oxidation of each fuel molecule, F is Faraday's constant, $D_{FUEL,EFF}$ is the effective diffusivity for the fuel in the porous anode, and δ is the thickness of the anode. The effective diffusivity for H_2 can be approximated using the Chapman-Enskog equation [24] along with values for the anode porosity and tortuosity which are estimated to be 0.35 and 3, respectively [23]. This gives an estimated value of $D_{H2,EFF}$ of 1.2 $cm^2\ s^{-1}$.

Equation 1 predicts that for the cells with 200 μm thick anodes, operating with a P_{H_2} at the surface of the anode of 0.1 atm (the lowest P_{H_2} used for these cells) at 973 K, a current density of ~1500 mA cm^{-2} is required for C_{TPB} to be only 10 % less than $C_{surface}$. Since this current density is significantly greater than the maximum current densities obtained from the Cu-CeO_2-YSZ and Ni-YSZ cells, this analysis shows that diffusional limitations did not affect performance. In order to demonstrate the validity of this analysis, experiments were conducted with a Cu-CeO_2-YSZ cell that was similar to the other Cu-ceria cell used in this study except that the anode was 3 mm in thickness (cell 4). With this

much thicker anode it was easier to operate under conditions for which diffusional limitations should occur. Figure 7 displays V-I curves and impedance spectra for cell 4 at 973 K as a function of P_{H_2}. For operation on humidified H_2 (3% H_2O) at 1 atm, the V-I curve is nearly linear with a maximum current of ~600 mA cm^{-2}. At this current density, equation 1 predicts that C_{TPB} is only 6% less than $C_{surface}$. Thus, as is observed experimentally, for this fuel concentration diffusional limitations would not be expected to have a significant affect on cell performance. When P_{H_2} is lowered to 0.05 atm by diluting in He, however, the V-I curve exhibits a large change in slope at ~200 mA cm^{-2} at which point the current density rapidly approaches a limiting value of 260 mA cm^{-2}. At this current density equation 1 predicts that C_{TPB} will be ~50 % less than $C_{surface}$. Since, as discussed earlier, the kinetics of the H_2 oxidation reaction on this anode are positive order in P_{H_2}, it is not surprising that a 50 % reduction in the fuel concentration at the TPB has a significant affect on cell performance. The data in Figure 7 also shows that changing the diluent from He to N_2 causes the switch to diffusional control to occur at a lower current density of 150 mA cm^{-2}. This is the expected result, since the higher mass of N_2 relative to H_2 would produce a slight decrease in the effective diffusivity.

The data in Figure 7 for operation of the cell on pure and diluted n-C_4H_{10} are also consistent with estimates of diffusional limitations based on equation 1. For n-butane, D_{eff} is estimated to be 0.1 cm^2 s^{-1} which is an order of magnitude lower than that for H_2. This decrease in D_{eff} relative to that for H_2, however, is roughly offset by the fact that for n-C_4H_{10} 26 electrons are produced per reaction compared to only 2 for H_2. Thus, for the same fuel partial pressure one would expect diffusional limitations for n-C_4H_{10} to become

apparent at nearly the same current densities as that for H_2. As shown in Figure 7 this is indeed the case.

4. Summary

In this study it was demonstrated that there are dramatic differences in the performance of Cu-CeO_2-YSZ and Ni-YSZ anodes when ruining on CO and syngas fuels. The Cu-CeO_2-YSZ composite anodes exhibited high activity for the electrochemical oxidation of H_2 and CO and similar performance was obtained for both of these fuels. It was even possible via the addition of a cobalt co-catalyst to produce Cu-CeO_2-based anodes that exhibited higher performance on CO compared to H_2. For example, a cell with a Cu-Co-CeO_2-YSZ anode and a relatively thick 60 μm YSZ electrolyte had maximum power densities of 310 and 370 mW cm^{-2} at 973 K when operating on H_2 and CO, respectively. The high activity of the Cu-CeO_2-based anodes for CO oxidation was in sharp contrast to that obtained for Ni-YSZ anodes. In agreement with previous reports it was found that while Ni-YSZ anodes have high activity for H_2 oxidation, they do not effectively catalyze the oxidation of CO and therefore exhibit poor performance when operating on this fuel. Thus, when operating Ni-YSZ anodes on dry syngas, only the H_2 component of the fuel is utilized.

Studies of the dependence of fuel concentration on cell performance also showed that the kinetics of the electrocatalytic oxidation of H_2 are positive order in P_{H_2} for Cu-CeO_2-YSZ anodes and nearly zero order for Ni-YSZ anodes. In contrast to previous

studies, dilution of H_2 by H_2O was found to have little effect of the anode kinetics for both Cu-CeO_2-YSZ and Ni-YSZ anodes.

Acknowledgments

We gratefully acknowledge the funding provided for this work by the Office of Naval Research and the Army's Coordinated Technology Alliance in Power and Energy.

References:

[1] M. Brown, S Primdahl, M. Moggensen, J. Electrochem. Soc., 147 (2000) 475-485.

[2] Y. Matsuzaki, I. Yasuda, J. Electrochem. Soc., 147 (2000) 1630-1635.

[3] K. Sasaki, Y. Hori, R. Kikuchi, K. Eguchi, A. Ueno, H. Takeuchi, M. Aizawa, K. Tsujimoto, H. Tajiri, H. Nishikawa, Y. Uchida, J. Electrochem. Soc., 149 (2002) 1630-1635.

[4] Y. Jiang, A.V. Virkar, J. Electrochem. Soc., 150 (2003) A942-A951.

[5] N. Sakai, K. Yamaji, T. Horita, Y.P. Xiong, H. Kishimoto, H. Yokokawa, *J.* Electrochem. Soc., 150 (2003) A689-A694.

[6] A S.P. Jiang, S.P.S. Badwal, Solid State Ionics, 123 (1999) 209-224.

[7] A. Ringuede, D. Bronine, J.R. Frade, Solid State Ionics, 146 (2002) 219-224.

[8] C. Wen, R. Kato, H. Fukunaga, H. Ishitani, K. Yamada, J. Electrochem. Soc., 147 (2003) 2076-2080.

[9] Z.T. Xia, S.H. Chan, K.A. Khor, Electrochemical and Solid State Letters, 7 (2004) A63-A65.

[10] R. J. Gorte, S. Park, J. M. Vohs, C. Wang, Adv. Mat, 12 (2000) 1465-1469.

[11] S. Park, R. J. Gorte, J. M. Vohs, J. Electrochem. Soc., 148 (2001) A443- A447.

[12] S. Park, R. Cracium, J.M. Vohs, R. J. Gorte, J. Electrochem. Soc., 146 (1999) 3603-3605.

[13] S. Park, J. M. Vohs, R. J. Gorte, Nature, 404 (2000) 265-267.

[14] S. Park, R. J. Gorte, J.M. Vohs, Applied Catalysis A, 200 (2000) 55-61.

[15] H. Kim, S. Park, J. M. Vohs, R. J. Gorte, J. Electrochem. Soc., 148 (2001) A693.

[16] H. Kim, J. M. Vohs, R. J. Gorte, J. of the Chemical Society, Chemical Communications (2001) 2334-2335.

[17] Y. Huang, J.M. Vohs, R J. Gorte, J. Electrochem. Soc., 151 (2004) A646-A651.

[18] Fuel Cell Handbook (6^{th} ed.), by EG&G Services Parson Inc, Science Applications International Corporation, Chapter 7 (2002) 4.

[19] GM. Pajonk, Applied Catalysis A: General, 202 (2000) 57-169.

[20] C. Lu, W. L. Worrell, J. M. Vohs, R. J. Gorte, J. Electrochem. Soc., 150 (2003) A1357-A1359.

[21] S. McIntosh, J. M. Vohs, R. J. Gorte, Electrochemical and Solid State Letters, 6 (2003) A240-A243.

[22] S.-I. Lee, J. M. Vohs, R. J. Gorte, J. Electrochem. Soc., 151 (2004) A1319-1323.

[23] O. Costa-Nunes, J. M. Vohs, R. J. Gorte, J. Electrochem. Soc., 150 (2003) A858-A863.

Figure Captions:

Figure 1. V-I curves and impedance spectra measured at 150 mA cm^{-2} for cells 1 and 2 operating at 973 K on the following pure fuels: (■) H_2, (●) CO, and (♦) syngas. Panel (A) is for cell 1 with the Cu-CeO_2-YSZ anode and panel (B) is for cell 2 with the Ni-YSZ anode.

Figure 2. V-I curves and impedance spectra measured at 150 mA cm^{-2} for cell 3 with a Cu-Co-CeO_2-YSZ anode operating at 973 K on (■) H_2, (●) CO, and (♦) syngas fuels.

Figure 3. V-I curves for cell 1 with a Cu-CeO_2-YSZ anode operating at 973 K on the following dry fuels: (■) H_2, (●) CO, and (▲) n-C_4H_{10}, and fuel mixtures: (■) 90% H_2/10% n-C_4H_{10} and (■) 90% CO/10 % n-C_4H_{10}.

Figure 4. Plots of voltage and anode overpotential versus current for the Cu-CeO_2-YSZ (cell 1) (A) and Ni-YSZ (cell 2) (B) anode cells as a function of P_{H_2} at 973 K. The P_{H_2O} in the fuel was held constant at 0.03 atm and the flow rates of H_2 and He were adjusted to give P_{H_2} values of (■) 0.97, (♦) 0.5, and (▲) 0.1 atm.

Figure 5. Plots of voltage and anode overpotential versus current for a Cu-ceria-YSZ anode cell (cell 1) operating at 973 K in (●) pure CO, (●) 50% CO diluted in N_2, and (♦) 50% CO diluted in CO_2.

Figure 6. V-I curves for cells with (A) Cu-CeO_2-YSZ (cell 1) (B) Ni-YSZ (cell 2) anodes operating at 1 atm and 973 K with a fuel containing 0.1 atm of H_2, (▲) 0, (▲) 0.03, and (Δ) 0.5 atm of H_2O, and the balance He. V-I curves obtained at 1073K are also shown for the Ni-YSZ cell for fuels containing 0.1 atm of H_2, (■) 0.03, (□) 0.5 atm of H_2O, and the balance He.

Figure 7. V-I curves for cell 4 with a 3 mm thick Cu-CeO_2-YSZ anode operating at 973 K in the following fuels: panel A, (■) humidified H_2 (3 % H_2O), (□) 5% humidified H_2 in He, and (■) 5% humidified H_2 in N_2, and panel B, (●) n-C_4H_{10}, (o) 5% n- C_4H_{10} in He, and (●) 5% n- C_4H_{10} in N_2.

Table 1 – Summary of the cells used in this study[1].

		Anode		Cathode[2]
Cell	Support	Composition (wt % of cermet)	Thickness (μm)/Area (cm^2)	Thickness (μm)/Area (cm^2)
1	Cathode	Cu (15) - CeO_2 (11)	200 / 0.35	600 / 0.785
2	Cathode	Ni (38)	200 / 0.35	600 / 0.785
3	Anode	Cu-Co (30) - CeO_2 (15)	300 / 0.785	60 / 0.35
4	Anode	Cu (30) - CeO_2 (15)	3000 / 0.785	60 / 0.35

[1] All cells had a 60 μm YSZ electrolyte.
[2] All cells had a LSF-YSZ composite cathode.

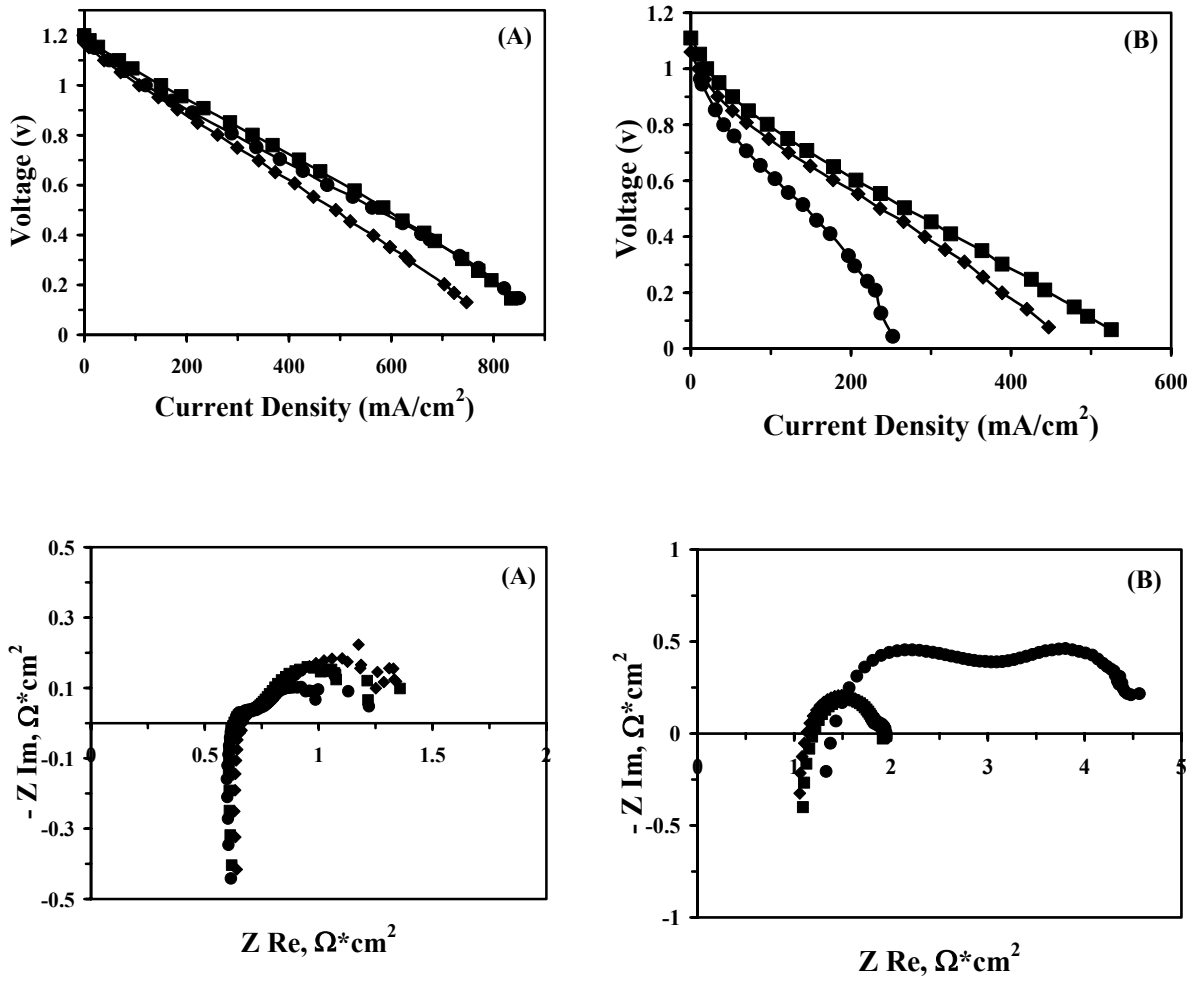
(A)
Voltage (v)
Current Density (mA/cm2)
(B)
Voltage (v)
Current Density (mA/cm2)
(A)
- Z Im, Ω*cm2
Z Re, Ω*cm2
(B)
- Z Im, Ω*cm2
Z Re, Ω*cm2

Figure 1.

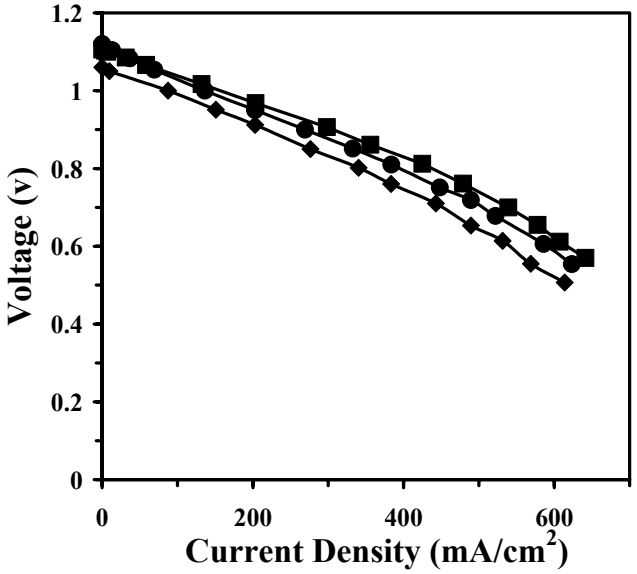
1.2
1
0.8
0.6
0.4
0.2
0
Voltage (v)
0
200
400
600
Current Density (mA/cm2)

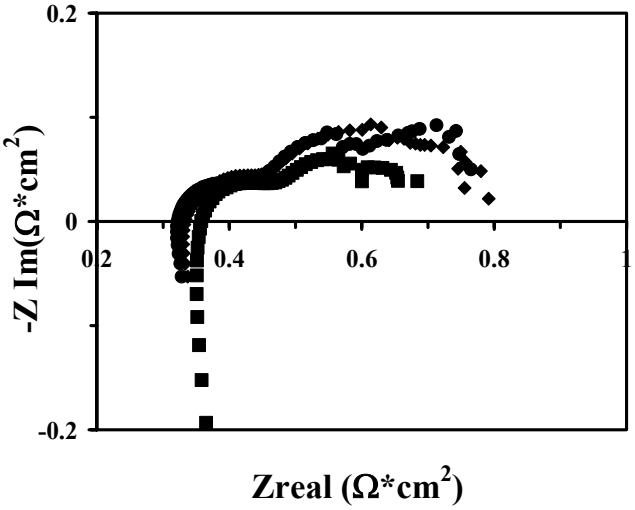
0.2
0
-0.2
-Z Im(Ω*cm2)
0.2
0.4
0.6
0.8
Zreal (Ω*cm2)

Figure 2.

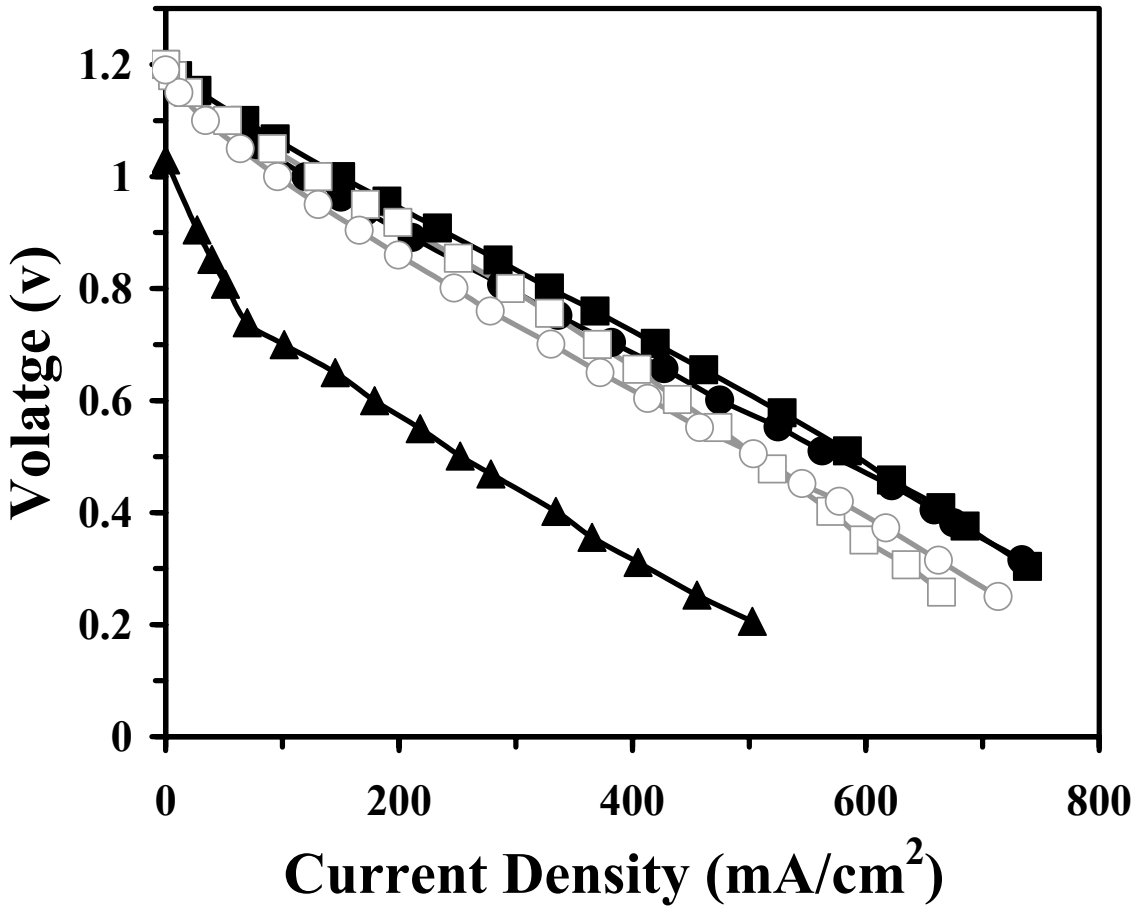
1.2
1
0.8
0.6
0.4
0.2
0
Volatge (v)
0
200
400
600
800
Current Density (mA/cm2)

Figure 3.

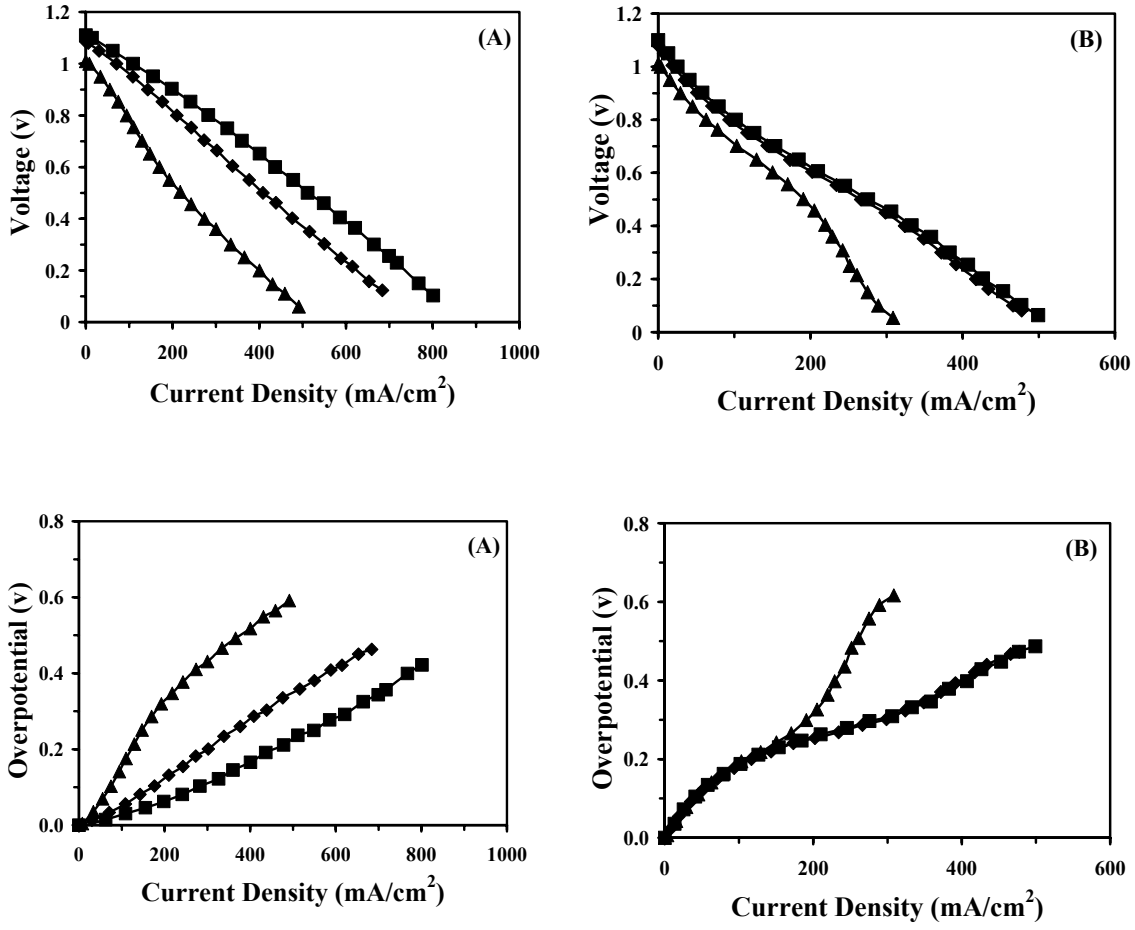
(A)
Voltage (v)
Current Density (mA/cm2)
(B)
Voltage (v)
Current Density (mA/cm2)
(A)
Overpotential (v)
Current Density (mA/cm2)
(B)
Overpotential (v)
Current Density (mA/cm2)

Figure 4.

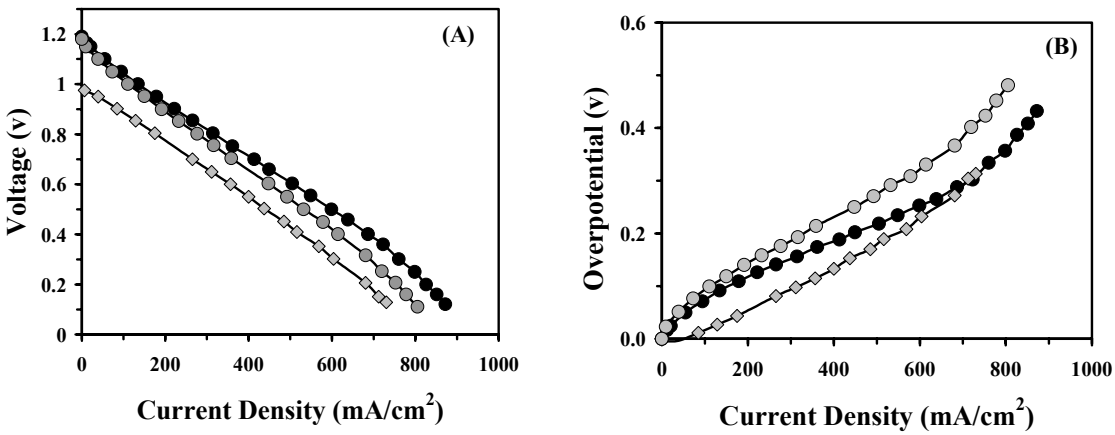
(A)
Voltage (v)
Current Density (mA/cm2)
(B)
Overpotential (v)
Current Density (mA/cm2)

Figure 5.

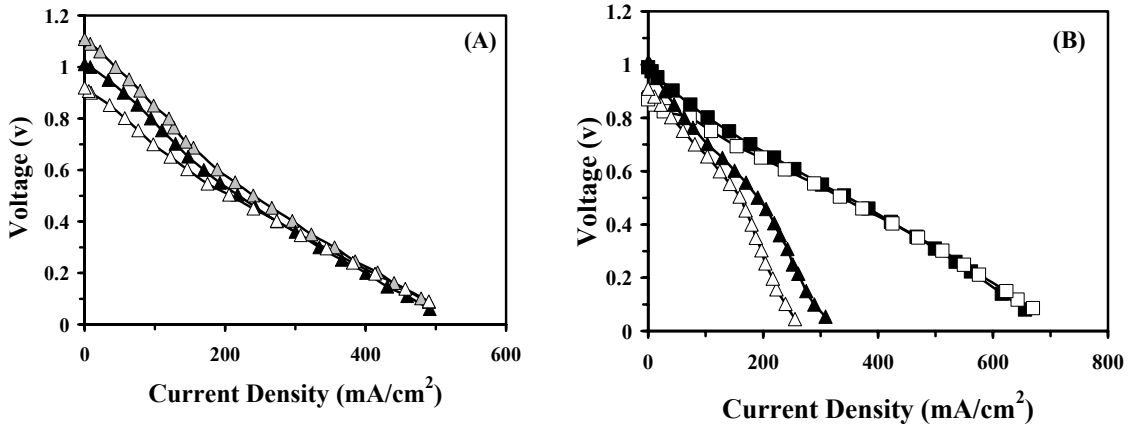
(A)
Voltage (v)
Current Density (mA/cm2)
(B)
Voltage (v)
Current Density (mA/cm2)

Figure 6

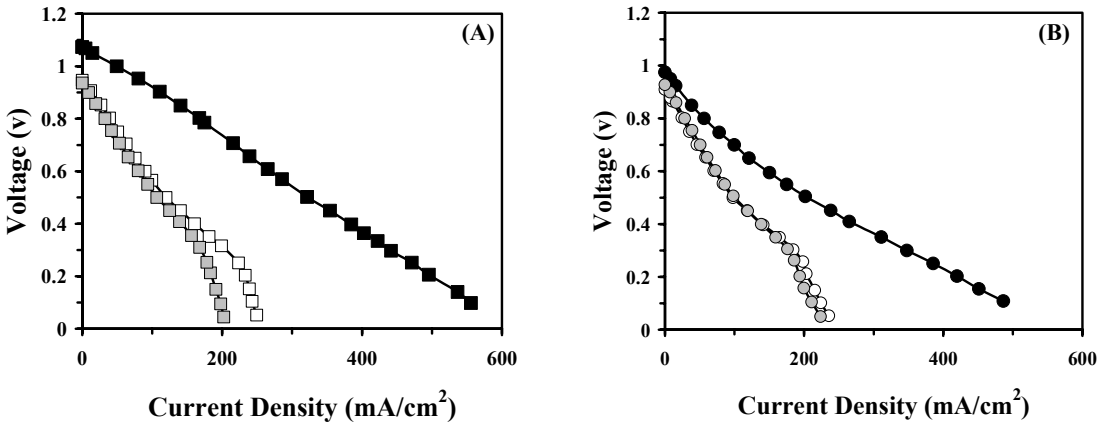
(A)
(B)
Voltage (v)
Current Density (mA/cm2)
1.2
1
0.8
0.6
0.4
0.2
0
0
200
400
600

Figure 7.